Ultramicroscopy 18 (1985) 335–348
North-Holland, Amsterdam

HREM STUDIES OF COHERENT AND INCOHERENT INTERFACES IN ZrO_2-CONTAINING CERAMICS: A PRELIMINARY ACCOUNT

A.H. HEUER, S. KRAUS-LANTERI, P.A. LABUN, V. LANTERI and T.E. MITCHELL

Department of Metallurgy and Materials Science, Case Western Reserve University, Cleveland, Ohio 44106, USA

Received 18 June 1985; presented at Symposium January 1985

HREM has been applied to the study of interfaces in various ZrO_2-containing ceramics. In dispersion-toughened ceramics, such as ZrO_2-toughened Al_2O_3, fine ZrO_2 particles can be either *intra-* or *inter-* granular. *Intra*granular ZrO_2 particles form *incoherent* interfaces with their Al_2O_3 hosts, and such interfaces have been imaged by HREM. The interfaces between *inter*granular ZrO_2 particles and Al_2O_3 grains are generally covered with a glassy phase, 1–3 nm in thickness, and evidence for this phase is also present in HREM images. If the ZrO_2 transforms from tetragonal to monoclinic symmetry during cooling from the fabrication temperature, it is generally twinned, and the *coherent* twin boundaries have also been imaged in HREM. Tetragonal precipitate colonies which occur on annealing certain ZrO_2–Y_2O_3 alloys have also been studied. Each colony consists of alternating variants which are 90° twins. HREM shows that the twin boundaries are highly coherent with a slight tilt between the variants. The "matrix" between the tetragonal colonies is shown by optical diffraction analysis of the HREM images to have tetragonal rather than cubic symmetry, indicating the occurrence of a diffusionless cubic → tetragonal transformation.

1. Introduction

ZrO_2-containing ceramics have attracted much attention in recent years because of their unusual mechanical and electrolytic properties [1,2]. Their considerable potential for high-technology structural applications derives from the phenomenon of *transformation toughening*. Briefly, ZrO_2 is polymorphic, the three polymorphs being shown in fig. 1 [3]. The high-temperature form is cubic and is isostructural with CaF_2 (fluorite structure). At temperatures below ≈ 2350°C for pure ZrO_2, or at temperatures considerably lower for ZrO_2 alloys, the cubic polymorph (c-ZrO_2) transforms to a tetragonally distorted version of the fluorite structure, shown in fig. 1b (t-ZrO_2). At still lower temperatures, t-ZrO_2 transforms martensitically to the monoclinic structure shown in fig. 1c (m-ZrO_2). This martensitic $t \rightarrow m$ transformation is the origin of transformation toughening in ZrO_2-containing ceramics, as will now be described.

In suitably fabricated ceramics, particularly if the t-ZrO_2 is present as fine particles, the start or M_s temperature of the martensitic transformation, which is ≤ 1000°C in pure bulk ZrO_2, can be reduced to below room temperature, i.e., the t-ZrO_2 is retained metastably at room temperature. However, the $t \rightarrow m$ transformation can be induced by external stresses, for example, the stress field associated with a propagating crack. This stress-induced tetragonal-to-monoclinic transformation thus "shields" the crack tip from the applied stresses and is the origin of the improved strength and toughness of transformation-toughened ZrO_2-containing ceramics.

It should be clear from this introduction that the type, amount, morphology and distribution of the ZrO_2 polymorphs within ZrO_2-containing ceramics are of prime importance, and both homophase (ZrO_2/ZrO_2) and heterophase (ZrO_2 particle/non-ZrO_2 matrix) interfaces are of interest. In fact, such studies of interfaces in polycrystalline, polyphase ceramics are crucial for understanding the variety of diffusional and diffusionless transformations that are important when considering microstructural evolution during fabrication and performance during service. Inasmuch as HREM can play a vital role in understanding

0304-3991/85/$03.30

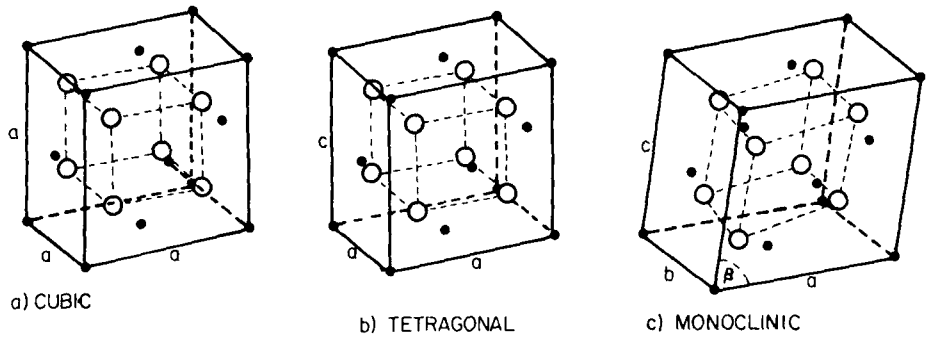

Fig. 1. Three polymorphs of ZrO_2: (a) cubic phase; (b) tetragonal phase, $c/a \approx 1.02$; (c) monoclinic phase. The small filled spheres are Zr atoms, the large open spheres are oxygen.

these technologically important ceramics, we have begun a broad program using high-resolution electron microscopy to study interfaces in such ceramics.

2. Experimental procedures

15 vol% ZrO_2-toughened Al_2O_3 (ZTA) specimens were obtained from Dr. N. Claussen (Max-Planck-Institut für Metallforschung, Stuttgart, Fed. Rep. of Germany). The starting powders were Alcoa A-16 Al_2O_3 and Magnesium Electron ARZ52 ZrO_2. Processing consisted of attritor milling for 12 h, followed by hot pressing at 1550°C for 30 min; the density of the resulting ceramic was 99.5% of theoretical.

Single crystal skull-melted ZrO_2-8 wt% Y_2O_3 was obtained from the Ceres Corporation. This material was then heat-treated for 50 h at 1600°C and furnace-cooled; Laue back-reflection photographs were used to orient the crystal to a $\langle 111 \rangle$ zone.

Both materials were prepared for TEM examination using standard techniques, i.e. diamond-wafering thin slices, grinding and polishing to approximately 50 μm thickness, followed by ion-beam thinning to electron transparency. A thin carbon coat was sputtered on one surface before insertion into a JEOL 200CX having a C_s of 1.1 mm and a point resolution of $\lesssim 0.24$ nm. An Intellect 200 image analysis system is used for on-line image processing; Skarnulis' CELLS program [4] is available for image simulation.

3. Zirconia-toughened alumina

ZTA, an example of a wider class of dispersion-toughened ceramics, is one of the three useful types of ZrO_2-containing ceramics. These materials typically contain 15 vol% ZrO_2 in a fine-grained Al_2O_3 matrix; the ZrO_2 can be *inter*- or *intra*granular and the propensity for undergoing the martensitic transformation depends markedly on the morphology of the ZrO_2 particles [5]. Furthermore, the stability of t-ZrO_2, i.e. its resistance to undergoing the martensitic transformation, involves stress concentrations at interfaces. It now appears that nucleation of the $t \rightarrow m$ martensitic transformation is always stress-assisted [6], and the magnitude of these stresses is very sensitive to particle morphology [7]. Understanding of the $t \rightarrow m$ martensitic transformation depends on increased knowledge of the interface structure, and a variety of ZrO_2–Al_2O_3 interfaces have been imaged with high-resolution electron microscopy.

The first example is shown in fig. 2. A roughly spherical m-ZrO_2 particle is completely enclosed within an Al_2O_3 grain. As has been discussed elsewhere [8], this morphology arises from "breakaway" grain growth of Al_2O_3 grain boundaries during densification or extended high-temperature

Fig. 2. Bright-field micrograph of intragranular ZrO_2 particle in Al_2O_3 grain.

annealing. While particles such as these are generally resistant to the martensitic transformation in bulk ceramics [5], foil preparation has been found to induce the $t \rightarrow m$ transformation, especially if, as in the present case, the ZrO_2 is free of any "stabilizer" solute. Thus, the ZrO_2 particle shown in fig. 2 has m symmetry, having transformed during foil preparation, and a conventional selected-area diffraction pattern of both the ZrO_2 particle and the Al_2O_3 matrix (not shown here) reveals the fortunate circumstance that the particle and matrix are oriented such that both are within a few degrees of a low-index zone axis orientation, [001] for ZrO_2 and [0001] for Al_2O_3. Furthermore, the foil is of relatively uniform thickness over the whole area of fig. 2, and could be imaged in HREM. A structure image of the ZrO_2 particle after tilting to the exact [001] orientation is shown in fig. 3, along with an image calculated by computer simulation. It is clear that the image matching in this particular instance is acceptable. We also hope to model the interfaces (at regions 1–4 in fig. 2 to be shown next), although such interface simulations have not yet been completed.

The particle–matrix interface is shown at higher resolution in fig. 4: the ZrO_2 is oriented exactly on the zone axis in fig. 4a, while the Al_2O_3 is oriented exactly on the zone axis in fig. 4b. The feature marked F in figs. 4a and 4b is a fault in the m-ZrO_2 which we have not yet analyzed. The

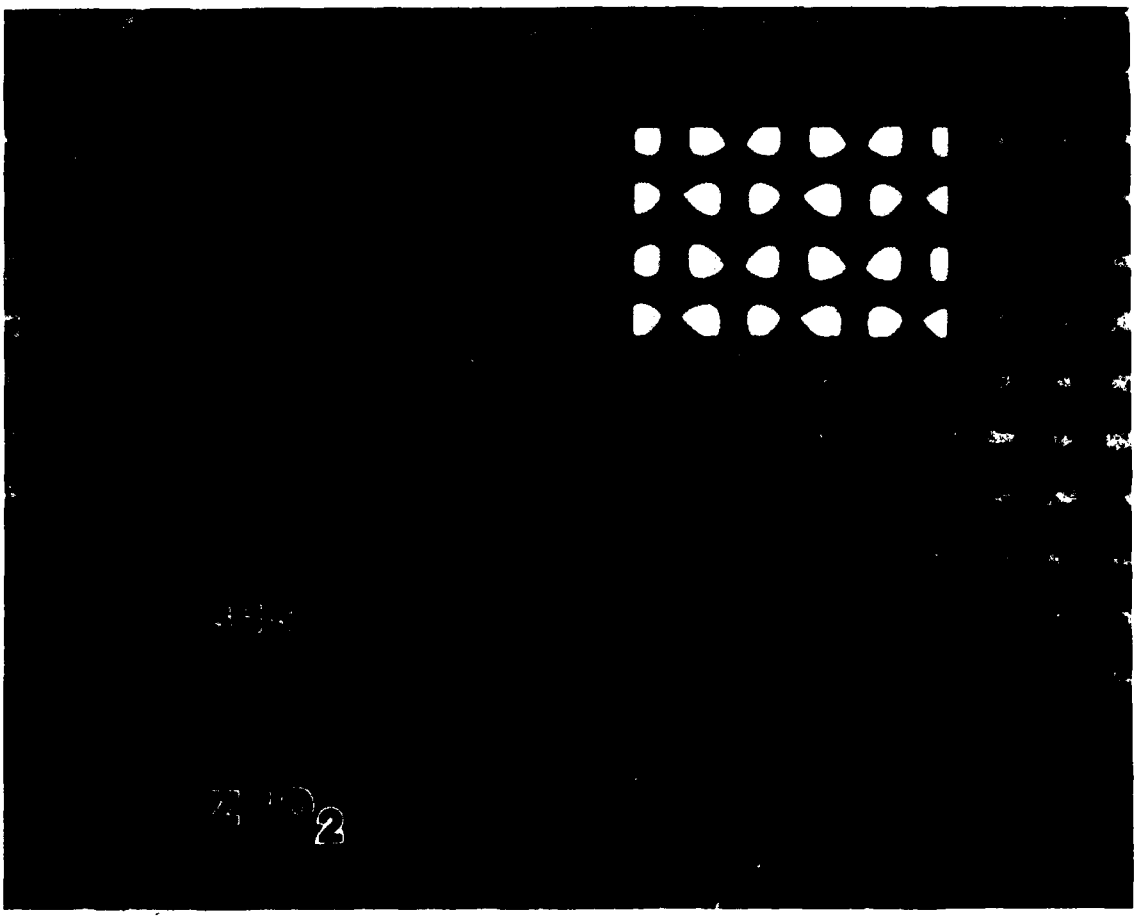

Fig. 3. High-resolution image of $[001]_m$ ZrO_2, with calculated image match. The unit cell is shown.

features marked 1 and 2 in fig. 4a denote particular interface regions which are shown at higher magnifications in fig. 5. We believe that the interface is most nearly parallel to the electron beam in region 1 in fig. 5a, and expect that sensible image interpretation of the atomic structure of this interface will be possible. On the other hand, the region shown in fig. 5b is judged to be uninterpretable because the interface is inclined to the electron beam; no further analysis is being contemplated for this image.

Slight tilting brings the Al_2O_3 grain into its symmetry position, and fig. 6 shows two regions (marked 3 and 4) on the opposite side of the faulted particle. Fig. 6a shows an area in which the interface is more or less parallel to the electron beam and for which we hope to provide suitable image simulations in the near future. Fig. 6b, on the other hand, shows a region of interface that is inclined to the electron beam and is judged unsuitable for further interpretation. Figs. 5a and 6a are remarkable in that they show the images extend right to the Al_2O_3–ZrO_2 interface, and that this *incoherent* interphase interface appears to accommodate the two dissimilar lattices without undue difficulty.

With regard to transformation toughening, intergranular particles are preferred in ZrO_2-

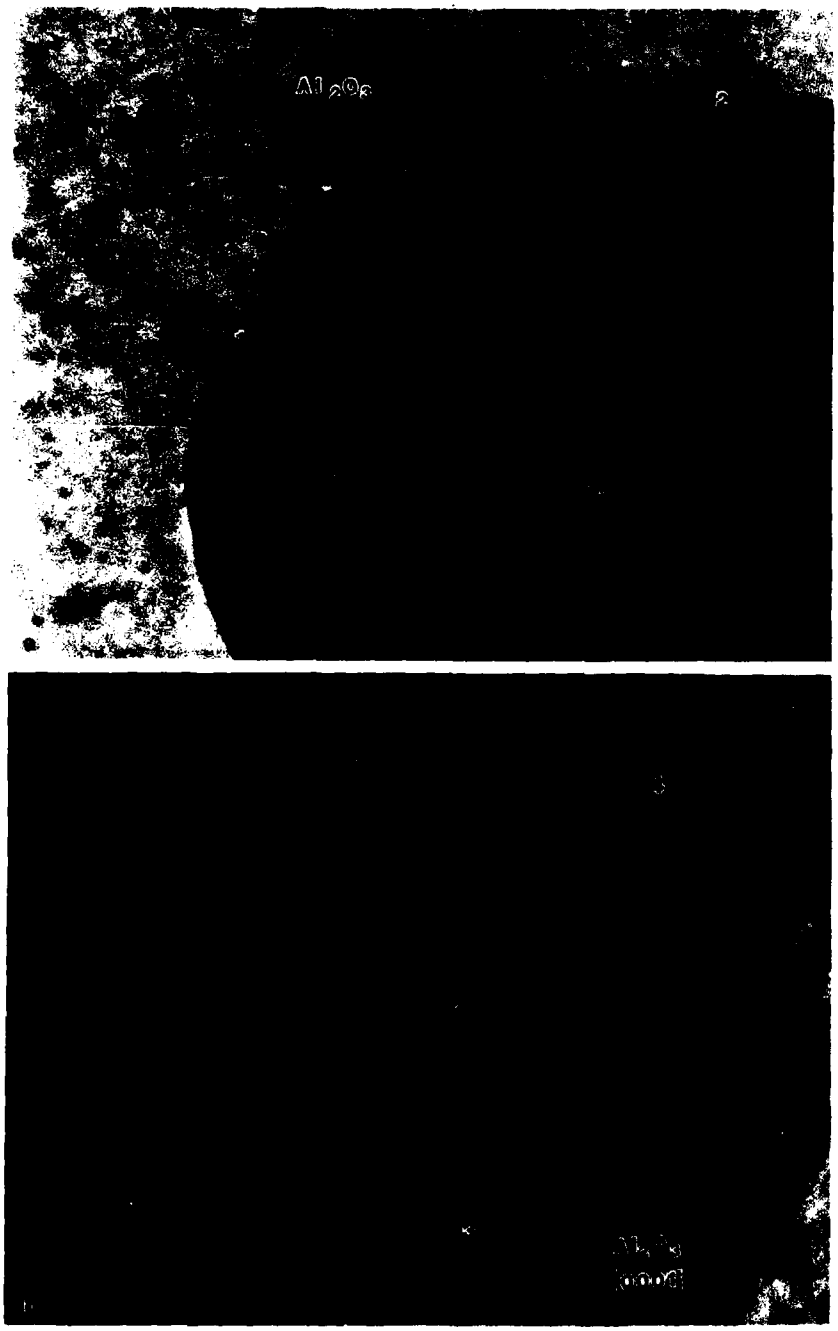

Fig. 4. (a) Higher-magnification micrograph of ZrO_2 particle in fig. 2 with interfacial regions 1 and 2 indicated. F is a fault in the particle. The foil is oriented so that ZrO_2 is exactly on the [001] orientation. (b) ZrO_2 particle with interfacial regions 3 and 4 indicated. The foil is oriented so that Al_2O_3 is exactly on the [0001] orientation.

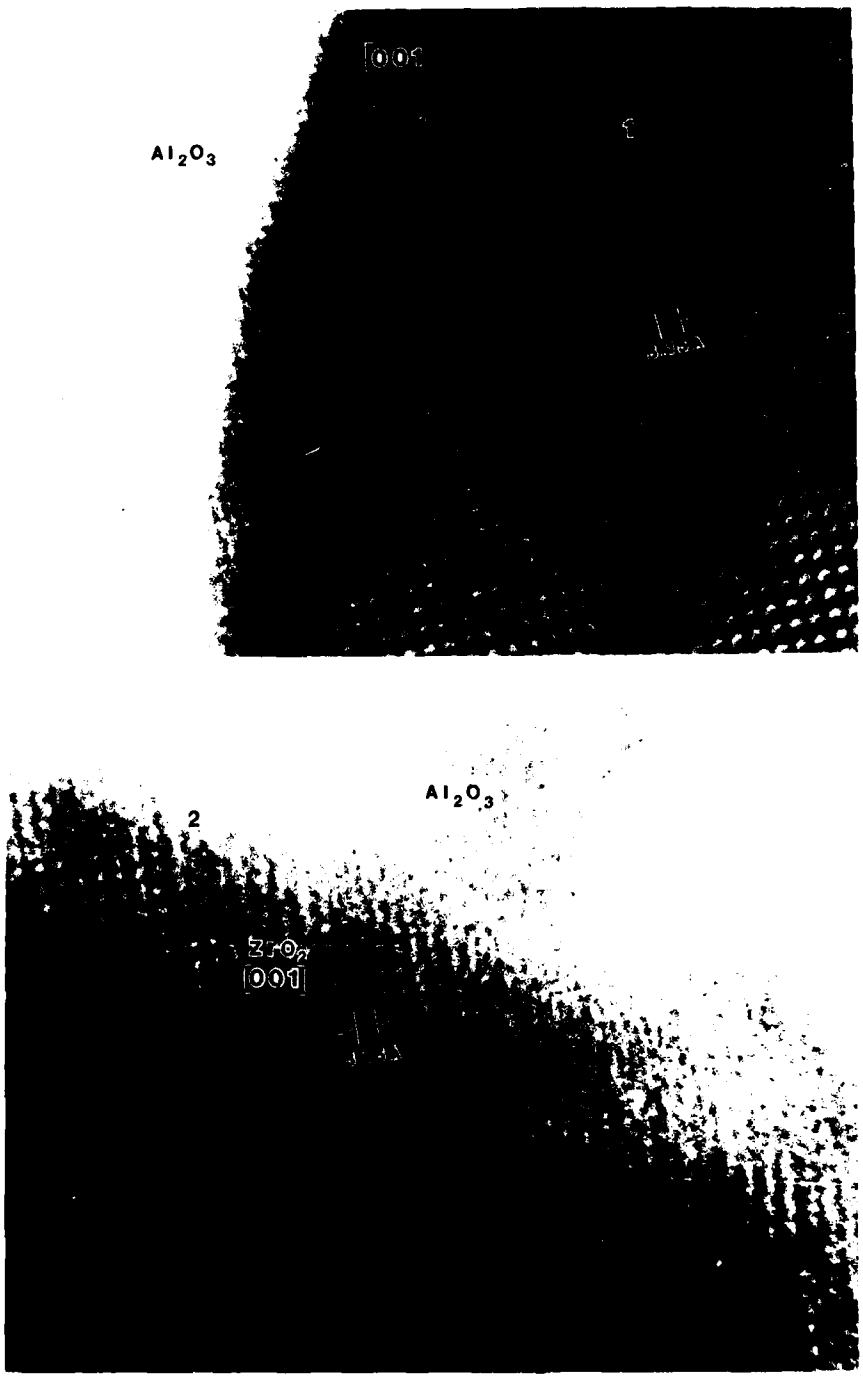

Fig. 5. (a) High-resolution image of interfacial region 1. (b) High-resolution image of interfacial region 2.

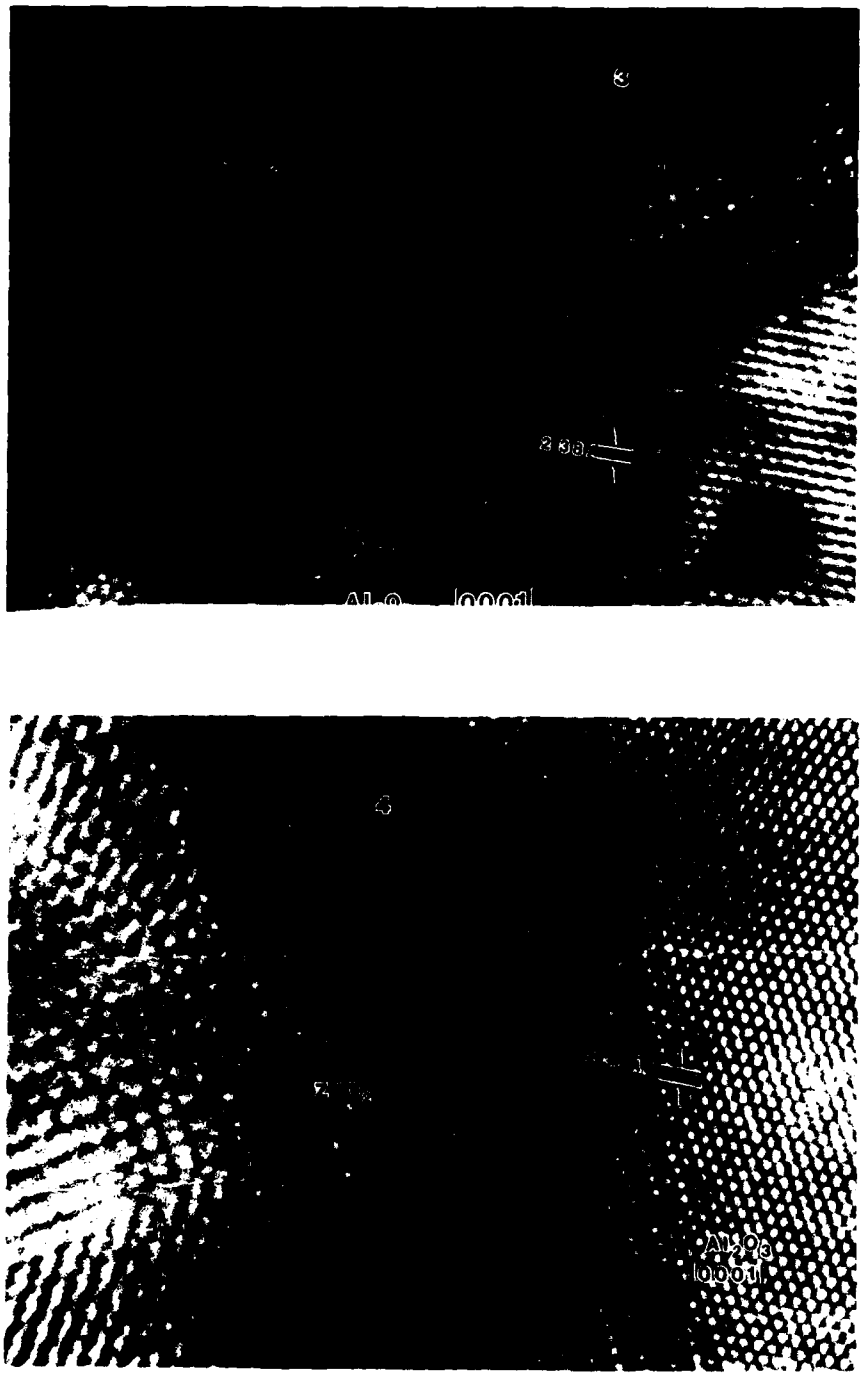

Fig. 6. (a) High-resolution image of interfacial region 3. (b) High-resolution image of interfacial region 4.

toughened Al_2O_3, and the sample of figs. 2–6 in fact contains more inter- than intragranular particles. However, it should be mentioned that virtually all Al_2O_3/Al_2O_3 grain boundaries and Al_2O_3/ZrO_2 intergranular boundaries in this sample are coated with a thin film (1–3 nm) of a SiO_2-containing amorphous phase (the SiO_2 impurity having been introduced during processing); such a grain boundary phase appears to be ubiquitous in all the ZrO_2-toughened Al_2O_3's studied to date. This glassy phase can best be imaged by forming a dark field image using diffuse inelastically scattered electrons. The glass is thus located at the bright regions in fig. 7 and the particular arrowed feature is glass along an Al_2O_3–Al_2O_3 grain boundary. The presence of such an amorphous phase at the Al_2O_3–ZrO_2 interface does not detract from detailed HREM studies of the interfaces. A HREM image of a twinned *m*-ZrO_2 particle in this sample is shown in fig. 8. (This is not the same region as shown in fig. 7.) The ZrO_2 particle is extensively twinned, the twinning occurring during spontaneous transformation on cooling following fabrication. This twinning occurs to minimize the shape strain of the particle during the martensitic transformation, and is present in virtually all *m*-ZrO_2 particles, except those which have transformed in a thin foil, as in fig. 2.

The orientations of the two Al_2O_3 grains and the several twinned "domains" of the ZrO_2 particle were determined by taking optical diffracto-

Fig. 7. Diffuse dark-field micrograph of intergranular ZrO_2 in an Al_2O_3 matrix, showing glassy phase at grain boundaries. (The arrowed region is an Al_2O_3/Al_2O_3 boundary.)

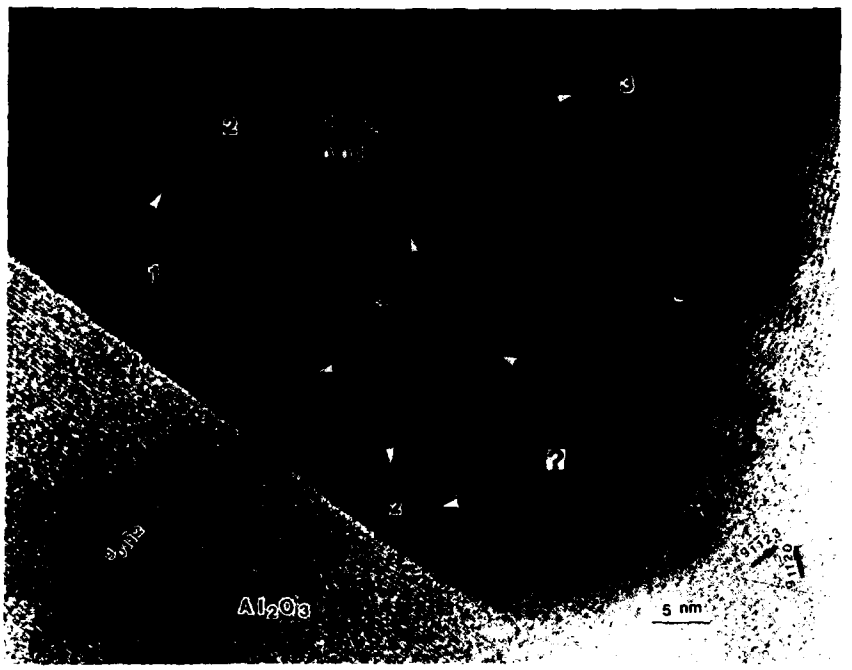

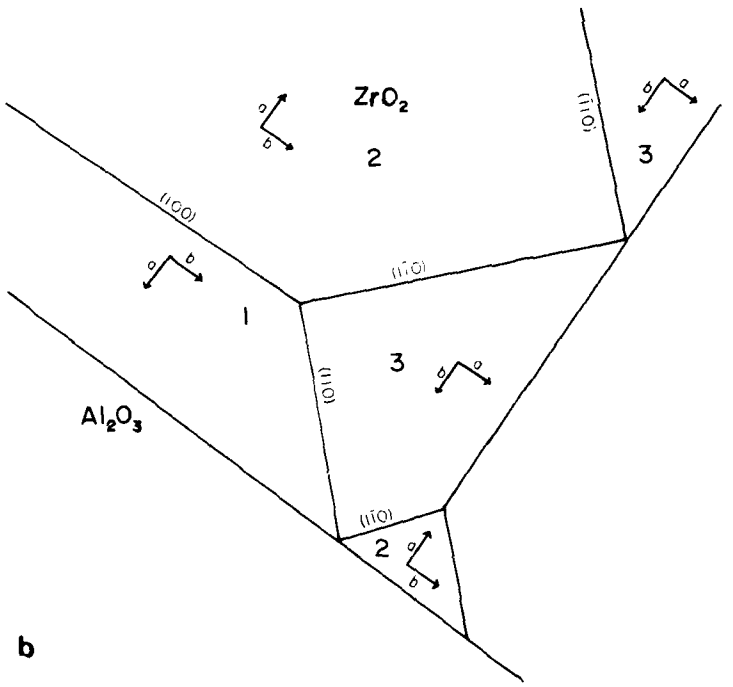

Fig. 8. (a) High-resolution image of intergranular ZrO_2 particle showing microtwins. The twin boundaries are arrowed, as is an Al_2O_3/Al_2O_3 grain boundary. 1, 2, and 3 refer to specific twin orientations shown in (b); the question-mark is a region of serious overlap between the ZrO_2 and Al_2O_3. (b) Diagram of (a) showing twin planes and orientations.

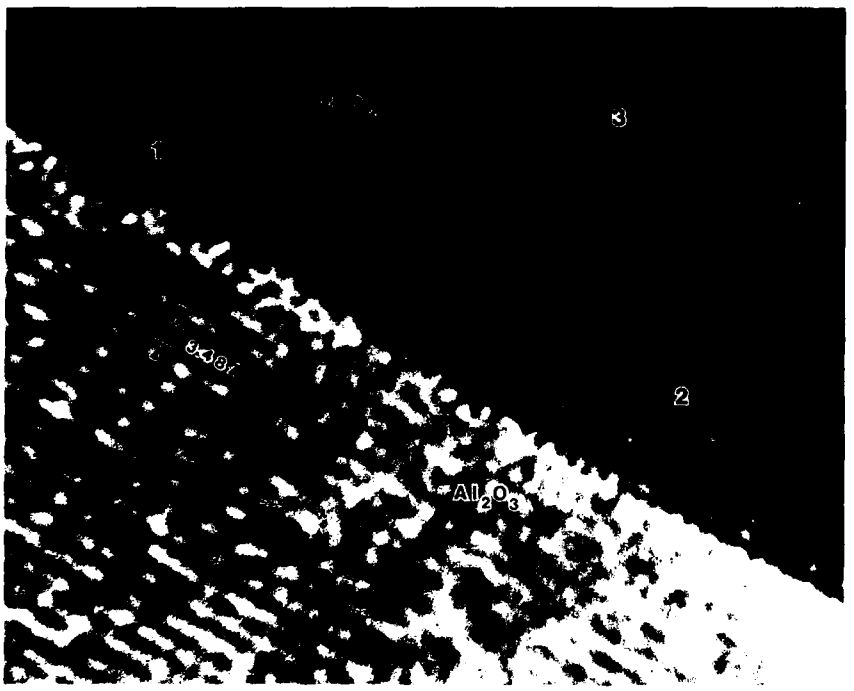

Fig. 9. High-resolution image of ZrO_2 particle in fig. 8a showing possible glassy phase at grain boundary. 1, 2, and 3 refer to the twin orientations shown in fig. 8b.

grams from fig. 8a, and yielded the results shown schematically in fig. 8b. The morphology of the twinned domains, as well as the existence of $(100)_m$, $(110)_m$, and $(1\bar{1}0)_m$ twin boundaries, are identical to the results described by Van Tendeloo et al. in ZrO_2–ZrN alloys [9].

The final figure for this section (fig. 9) shows the Al_2O_3–ZrO_2 interface at high magnification. It is tempting to argue that the broad bright region between the Al_2O_3 and ZrO_2 is a manifestation of the amorphous phase believed to be present, but image simulation is clearly needed to resolve this point. Even lacking such image simulation, it is again remarkable that the features in the structure image extend virtually undisturbed to the incoherent interphase interface. (It is fortunate that the interface in this region of foil is essentially parallel to the electron beam.)

4. ZrO_2–Y_2O_3 alloys

ZrO_2–Y_2O_3 alloys represent a second major class of ZrO_2-containing ceramics which have also been subject to significant commercial exploitation. Low Y_2O_3-content (2–4 mol%) compositions in this system are in use as strong and tough wear-resistant ceramics [10]; medium Y_2O_3-content (4–8 mol%) compositions find use as oxygen sensors in automotive application [11]; and single crystals containing ~ 10 mol% Y_2O_3 are used as imitation diamonds [12]. We have been studying phase equilibria at temperatures between 1300 and 1600°C in this system using a range of compositions between 3 and 9 mol% Y_2O_3. Our strategy is to anneal various compositions for long times to allow the pro-eutectoid precipitation reaction to go to completion and to use analytical electron mi-

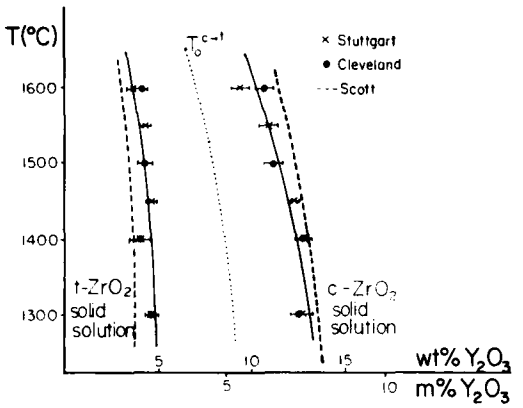

Fig. 10. ZrO_2-rich portion of the equilibrium phase diagram in the ZrO_2-Y_2O_3 system. The equilibrium compositions were determined by EDS methods.

croscopy to study the compositions of the coexisting c and t solid solutions (Y_2O_3 is very potent in stabilizing t-ZrO_2 and reducing M_s well below room temperature) [3]. The results of these AEM studies are shown in the partial phase diagram in fig. 10 [3]. For most compositions in the two-phase $t + c$ solid solution phase field, the t-ZrO_2 occurs as twinned "colonies", whose structure will be discussed in the remainder of this paper. The colony structure is shown in fig. 11a; this micrograph is taken from a 4 mol% Y_2O_3-ZrO_2 single crystal oriented to an exact ⟨111⟩ matrix zone-axis orientation. Each colony contains two t variants, which are actually 90° twins (fig. 11b); this morphology occurs to minimize strain between the colony precipitates and the matrix. As will be discussed next, the matrix also has tetragonal sym-

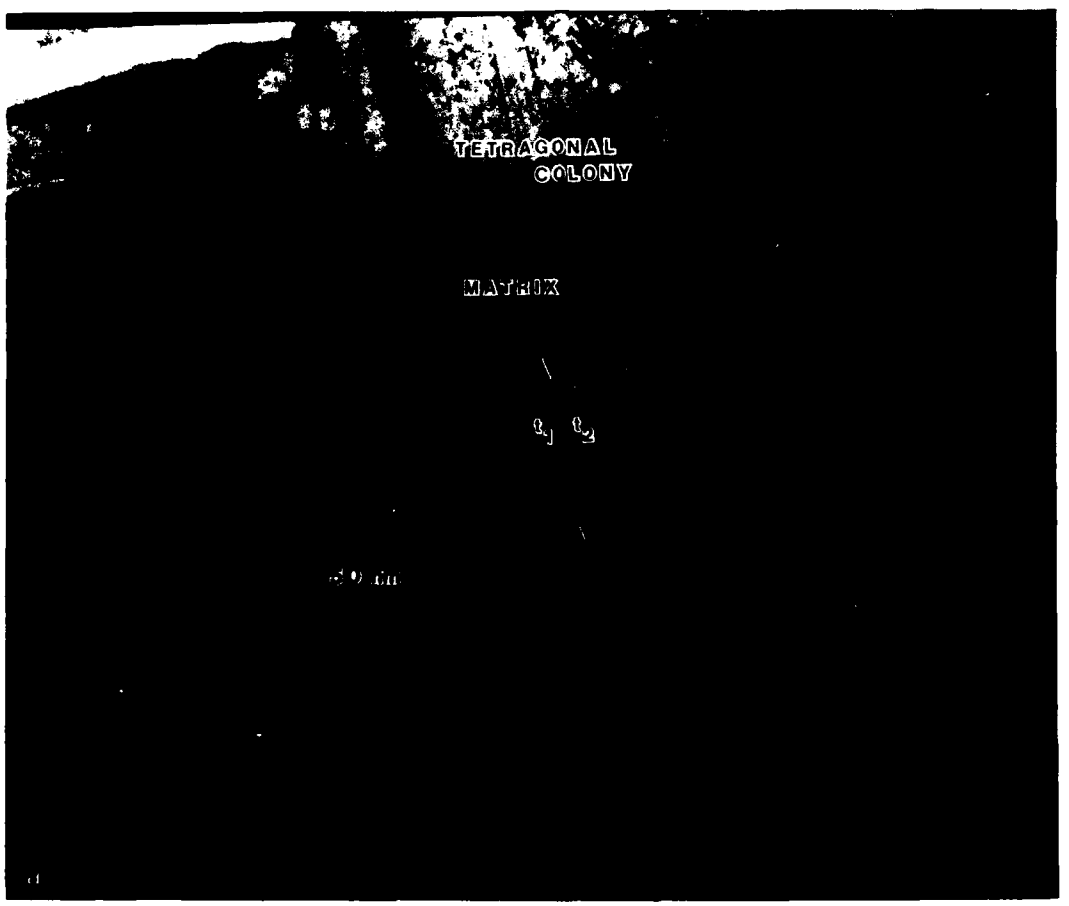

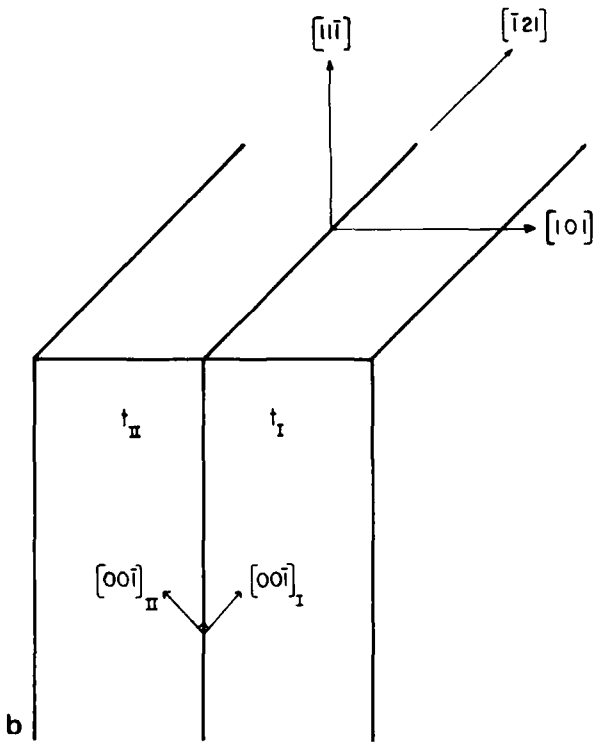

Fig. 11. (a) Tetragonal colony structure in ZrO_2–4 mol% Y_2O_3 showing a typical interface of interest (arrowed). (b) Schematic diagram showing twin variant crystallography. (The interface is perpendicular to [101].)

metry, having undergone a diffusionless $c \rightarrow t$ transformation on cooling from the annealing temperature [3]. The twinned colony structure of the t-ZrO_2 precipitates is very stable even during extended annealing; the number of twins per colony remains constant even as the colonies coarsen [13].

A HREM image of a twin variant interface is shown in fig. 12; this interface is similar to the one arrowed in fig. 11a, but of course was taken in a thinner region of the foil. It can be seen that the (1$\bar{1}$0) planes are imaged in one t variant, while the (2$\bar{2}$0) planes are imaged in its twin. This difference is believed to result from the very small tilt of one twin relative to the other, and would not occur were the c/a ratio exactly unity.

The origin of the colony stability is also apparent from fig. 12. The twin interface of fig. 12 (marked TB) can hardly be discerned; were it not for the slight tilt of the two twins, the twin boundary might not be visible. The good atomic matching thus implied assures that the twin boundary energy is correspondingly low. Thus, interface energy in the twinned structure must always be less than the reduced strain energy between colony precipitate and matrix.

The HREM study has also helped resolve a question concerning the matrix crystallography. As first suggested by Scott [14], and as is discussed elsewhere [3,13,15], c-ZrO_2 alloys quenched from high temperature can undergo a displacive $c \rightarrow t$ transformation below a certain critical temperature, T_0. (The variation in T_0 with composition is indicated by the dashed line in fig. 10 marked $T_0^{c \rightarrow t}$.) The equilibrium composition of the c-ZrO_2 matrix annealed at 1600°C is 6.0 mol% Y_2O_3; T_0 for this composition is ~ 900°C. We thus expect both the matrix and the colonies of fig. 11 to have t symmetry, but to differ in Y_2O_3 content by a

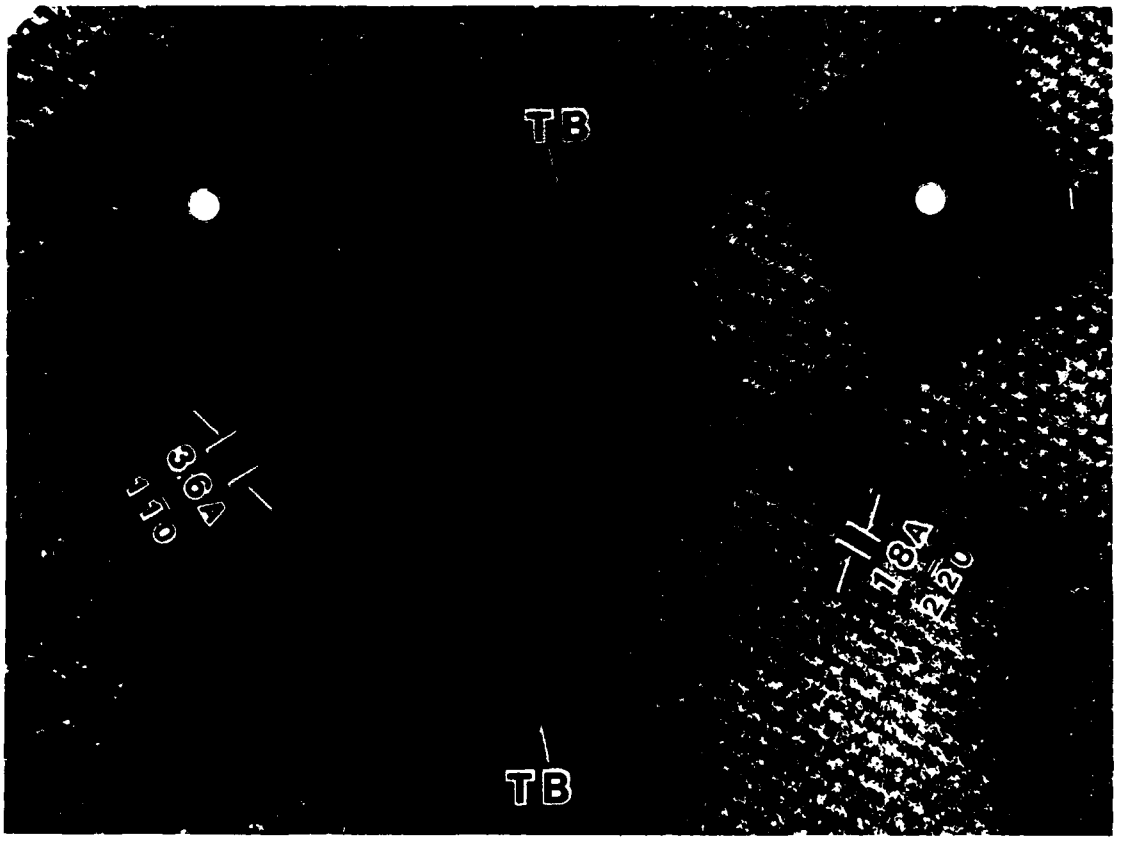

Fig. 12. High-resolution image of a coherent twin boundary (TB) between two tetragonal variants within the same colony. Optical diffractograms are shown as inserts.

factor of ~ 3. This chemical difference has been confirmed by AEM [13]. However, the variation in lattice parameter with Y_2O_3 solute is too small in this system to give rise to any spot splitting in the *odd, odd, even* reflections unique to t-ZrO_2 in conventional large-area SAD patterns, and it is difficult to be certain that there is no contribution from the colonies in any SAD pattern taken only from the matrix.

Fig. 13 shows a high-resolution image of the matrix, along with two optical diffractograms taken from different regions of the image. The {220} planes with 0.18 nm spacing imaged on the left portion of fig. 13 are consistent with either c or t symmetry. Slight bending of the foil has caused the adjacent area to be slightly off the exact orientation. In this region, (110) planes with 0.36 nm spacing are being imaged. (110) is a forbidden reflection for both c-ZrO_2 and t-ZrO_2, but often occurs in t-ZrO_2 by double diffraction from (112) planes. In any event, this spacing in the optical diffraction pattern is unambiguous evidence that the matrix has undergone the $c \rightarrow t$ transformation.

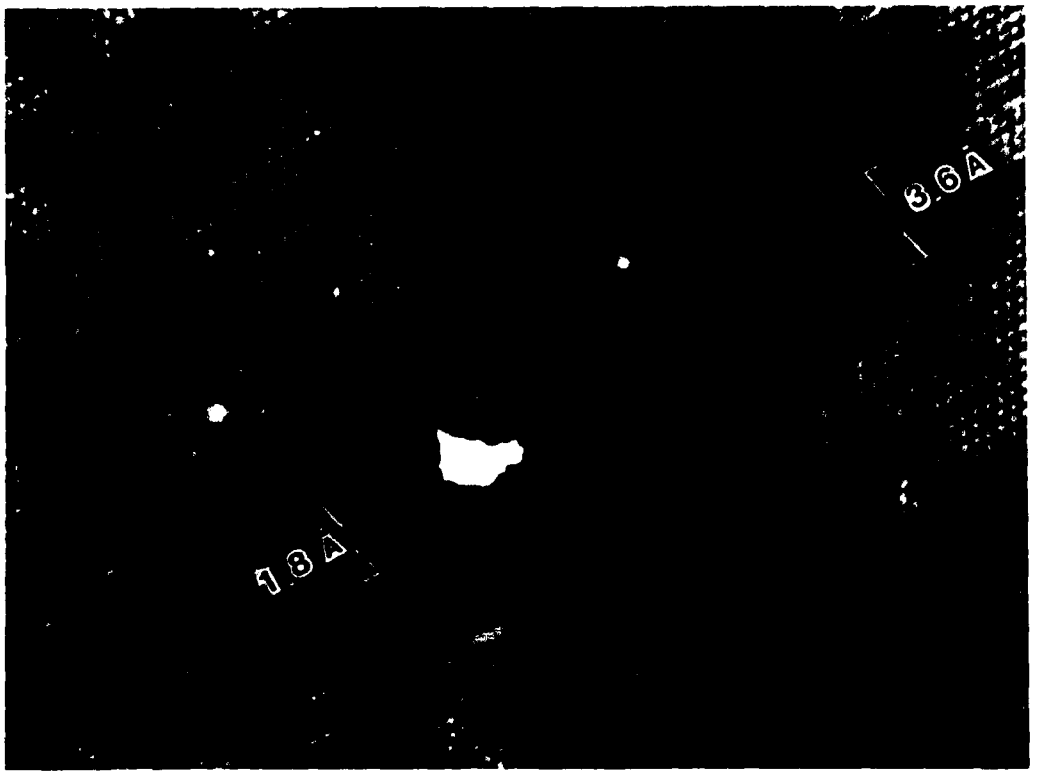

Fig. 13. High-resolution image and optical diffractograms of the matrix between two colonies.

Acknowledgments

This research was support by the Air Force Office of Scientific Research, Grant No. AFOSR-82-0227. We also gratefully acknowledge the National Science Foundation who provided the funds to establish our HREM facility.

References

[1] A.H. Heuer and L.W. Hobbs, Eds., Science and Technology of Zirconia, Advances in Ceramics, Vol. 3 (American Ceramic Society, Columbus, OH, 1981).
[2] N. Claussen, M. Rühle and A.H. Heuer, Eds., Science and Technology of Zirconia II, Advances in Ceramics, Vol. 12 (American Ceramic Society, Columbus, OH, 1984).
[3] A.H. Heuer and M. Rühle, ref. [2], p. 1.
[4] A.J. Skarnulis, J. Appl. Cryst. 12 (1979) 636.
[5] A.H. Heuer, N. Claussen, M.W. Kriven and M. Rühle, J. Am. Ceram. Soc. 65 (1982) 642.
[6] A.H. Heuer and M. Rühle, Acta Met., in press.
[7] S. Schmauder, W. Mader and M. Rühle, ref. [2], p. 126.
[8] B.W. Kibbel and A.H. Heuer, ref. [2], p. 260.
[9] G. Van Tendeloo, L. Anders and G. Thomas, Acta Met. 31 (1983) 1619.
[10] M. Rühle, N. Claussen and A.H. Heuer, ref. [2], p. 360.
[11] E.M. Logothestis, ref. [1], p. 388.
[12] E.C. Subbarao, ref. [1], p. 1.
[13] V. Lanteri, T.E. Mitchell and A.H. Heuer, ref. [2], p. 187.
[14] H.G. Scott, J. Mater. Sci. 10 (1975) 1527.
[15] R. Chaim, M. Rühle and A.H. Heuer, J. Am. Ceram. Soc. 68 (1985) 427.